Journal of Structural Biology 216 (2024) 108113

Contents lists available at ScienceDirect

Journal of Structural Biology

journal homepage: www.elsevier.com/locate/yjsbi

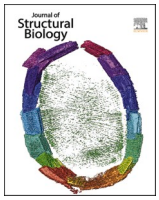

Structure Report

Crystal structure of the GluK1 ligand-binding domain with kainate and the full-spanning positive allosteric modulator BPAM538

Yasmin Bay [a], Federico Javier Miguez Cabello [b], Chloe C. Koens [c], Stine M. Frantsen [a], Darryl S. Pickering [a], Karla Frydenvang [a], Pierre Francotte [d], Bernard Pirotte [d], Anders S. Kristensen [a], Derek Bowie [b], Jette Sandholm Kastrup [a,*]

[a] Department of Drug Design and Pharmacology, Faculty of Health and Medical Sciences, University of Copenhagen, DK-2100 Copenhagen, Denmark
[b] Department of Pharmacology and Therapeutics, McGill University, Montreal, Quebec, Canada
[c] Integrated Program in Neuroscience, McGill University, Montreal, Quebec, Canada
[d] Department of Medicinal Chemistry, Center for Interdisciplinary Research on Medicines (CIRM), University of Liège, Liège, Belgium

ARTICLE INFO

Keywords:
X-ray crystallography
Ligand-binding domain of GluK1
Positive allosteric modulator
Kainate
Binding mode

ABSTRACT

Kainate receptors play an important role in the central nervous system by mediating postsynaptic excitatory neurotransmission and modulating the release of the inhibitory neurotransmitter GABA through a presynaptic mechanism. To date, only three structures of the ligand-binding domain (LBD) of the kainate receptor subunit GluK1 in complex with positive allosteric modulators have been determined by X-ray crystallography, all belonging to class II modulators. Here, we report a high-resolution structure of GluK1-LBD in complex with kainate and BPAM538, which belongs to the full-spanning class III. One BPAM538 molecule binds at the GluK1 dimer interface, thereby occupying two allosteric binding sites simultaneously. BPAM538 stabilizes the active receptor conformation with only minor conformational changes being introduced to the receptor. Using a calcium-sensitive fluorescence-based assay, a 5-fold potentiation of the kainate response (100 μM) was observed in presence of 100 μM BPAM538 at GluK1(Q)$_b$, whereas no potentiation was observed at GluK2(VCQ)$_a$. Using electrophysiology recordings of outside-out patches excised from HEK293 cells, BPAM538 increased the peak response of GluK1(Q)$_b$ co-expressed with NETO2 to rapid application of 10 mM L-glutamate with 130 ± 20 %, and decreased desensitization determined as the steady-state/peak response ratio from 23 ± 2 % to 90 ± 4 %. Based on dose–response relationship experiments on GluK1(Q)$_b$ the EC_{50} of BPAM538 was estimated to be 58 ± 29 μM.

1. Introduction

The ionotropic glutamate receptors (iGluRs) are involved in most of the fast excitatory synaptic transmission in the central nervous system. The iGluRs are categorized into four receptor subfamilies: AMPA, kainate, NMDA, and delta receptors (Hansen et al., 2021). This class of receptors is important for learning and memory formation but is also entangled in the development of neurological diseases. The kainate receptors are believed to mediate both a postsynaptic excitatory response and a modulatory presynaptic response, leading to modulation of the release of the inhibitory neurotransmitter GABA (Lerma & Marques, 2013). Kainate receptors have also been associated with neurological diseases such as epilepsy, schizophrenia, and depression (Lerma & Marques, 2013).

The kainate receptors comprise five subunits, termed GluK1-5. While the subunits GluK1-3 may form functional homo- and hetero-tetrameric receptors, subunits GluK4-5 can only form functional receptors with GluK1-3 (Contractor et al., 2011). The topology of a single subunit is

Abbreviations: AMPA, α-amino-3-hydroxy-5-methylisoxazole-4-propionate; DMSO, dimethyl sulfoxide; GluK1-LBD, ligand-binding domain of GluK1; iGluRs, ionotropic glutamate receptors; LBD, ligand-binding domain; L-Glu, L-glutamate; PAMs, positive allosteric modulators; Pk, peak response; RFU, relative fluorescence unit; SS, steady-state.

* Corresponding author.
E-mail address: jsk@sund.ku.dk (J.S. Kastrup).

https://doi.org/10.1016/j.jsb.2024.108113
Received 20 November 2023; Received in revised form 4 July 2024; Accepted 26 July 2024
Available online 28 July 2024

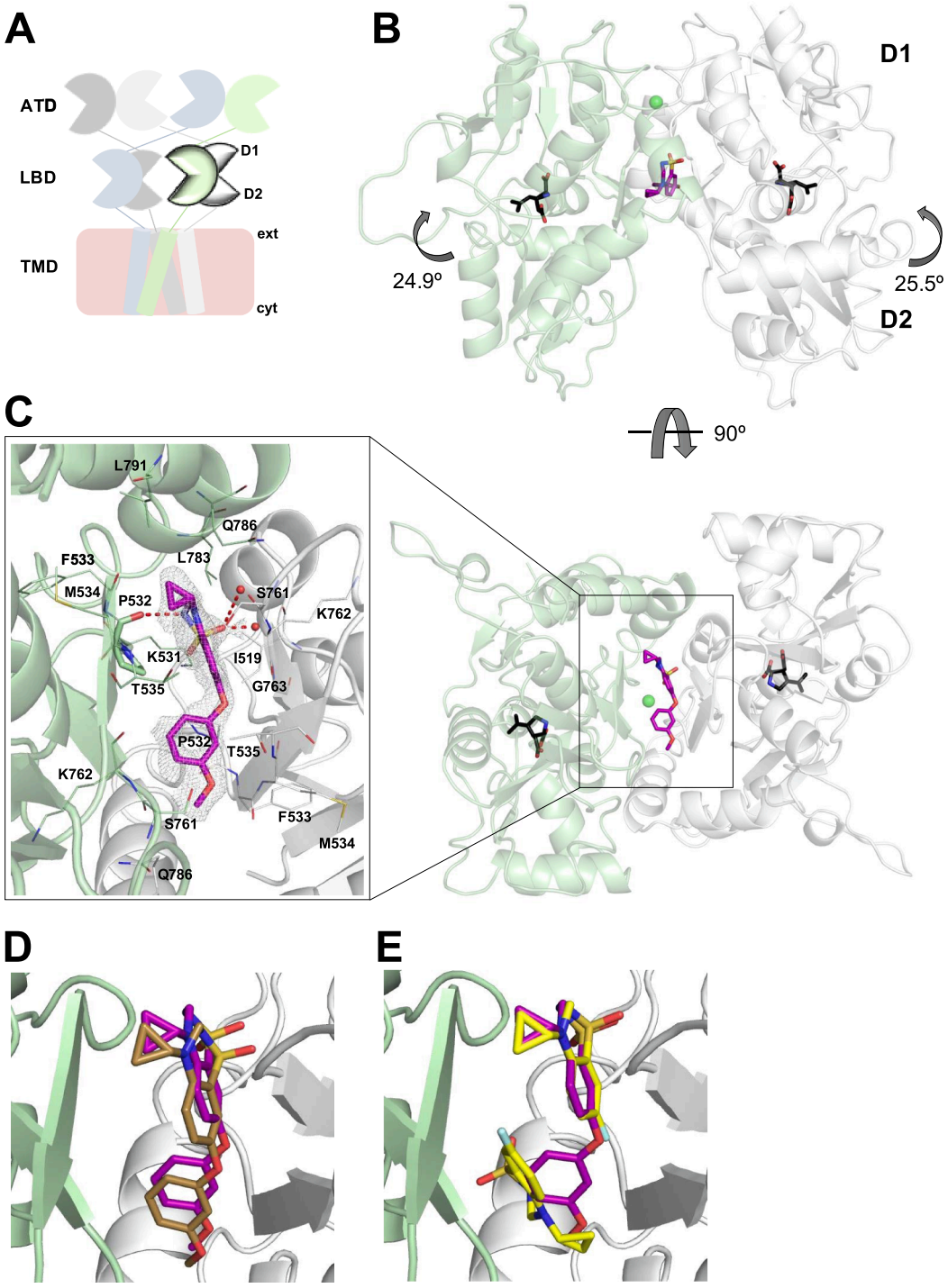

Fig. 1. Crystal structure of GluK1-LBD in complex with the agonist kainate and the positive allosteric modulator BPAM538. (A) Schematic drawing of a full-length kainate receptor. From the top: the amino-terminal domain (ATD) and underneath the ligand-binding domain (LBD) harboring the binding site of L-Glu and other ligands. The LBD resembles a clamshell structure with an upper lobe D1 and a lower lobe D2. The transmembrane domain (TMD, simplified) is embedded in the membrane and connected to a carboxy-terminal domain (CTD; not shown). (B) Dimer views: side (top panel) and bottom (bottom panel) of the GluK1-LBD structure with kainate and BPAM538. Chains A (pale green) and B (grey) are shown in cartoon representation. Kainate and BPAM538 are shown in sticks representation with carbon atoms colored black and purple, respectively. One chloride ion is shown as a green sphere. (C) Close-up on the lower part of the dimer interface where one BPAM538 molecule binds, presented with the $2F_o$-F_c omit electron density map contoured at 1 sigma and carved at 1.9 Å. Residues within 4 Å of BPAM538 are shown as lines, and water molecules as red spheres. Hydrogen bonding interactions (<3.5 Å) between BPAM538 and the residue P532 or water molecules are highlighted as red stippled lines. Oxygen atoms are red, nitrogen atoms blue, and sulfur atoms yellow. (D) Superimposition of GluK1-LBD (kainate and BPAM538) and GluA2-LBD (L-Glu and BPAM538; PDB code: 5OEW) structures on lobe D1 residues. GluK1-LBD is shown in cartoon representation, whereas GluA2-LBD has been left out for clarity. BPAM538 is seen to bind in a very similar manner in GluK1 (magenta) and GluA2 (brown). (E) Superimposition of GluK1-LBD (kainate and BPAM538) and GluK1-LBD (kainate and BPAM344; PDB code: 5MFQ) structures on lobe D1 residues. BPAM538 is seen to overlay with one of the two BPAM344 molecules (represented in yellow). Only the protein chain of the structure with BPAM538 is shown. (For interpretation of the references to colour in this figure legend, the reader is referred to the web version of this article.)

composed of four distinct domains that share common structural features with the other iGluR subfamilies (Sobolevsky et al., 2009; Hansen et al., 2021) (Fig. 1A). Among the iGluRs, the physiological role of kainate receptors is less well understood and tool compounds with subtype selectivity are sparse. Understanding the molecular function of kainate receptors may help unravel their potential as targets for treating neurological diseases by discovering selective tool compounds.

Allosteric modulators are generally thought to be better tolerated as they modify existing levels and patterns of receptor activation rather than constitutively blocking or over-activating all receptors. Additionally, allosteric modulators have a higher potential for receptor subtype selectivity as they often target less conserved regions than the orthosteric binding site (Traynelis et al., 2010). These allosteric regions are typically more hydrophobic compared to orthosteric sites, providing a physicochemical ligand space that is more optimal for entering the central nervous system, e.g., requiring a lower number of H-bonds acceptors/donors (Tee & Berezovsky, 2024). Whereas many small molecule positive allosteric modulators (PAMs) of AMPA receptors exist, only a few PAMs for kainate receptors have been reported (Larsen et al., 2017; Puja et al., 2022). These PAMs belong to class II, which bind with two molecules at the dimer interface between two ligand-binding domains (LBDs) within the receptor (Larsen et al., 2017; Frydenvang et al., 2022). PAMs exert their effect by decreasing desensitization and/or deactivation of the receptor, thereby enhancing receptor activation by L-glutamate (L-Glu) through binding to the allosteric site (Jin et al., 2005; Sun et al., 2002).

4-Cyclopropyl-7-(3-methoxyphenoxy)-3,4-dihydro-2*H*-1,2,4-benzothiadiazine 1,1-dioxide (BPAM538; Fig. 2) was previously reported to be a highly potent PAM at AMPA receptors with nanomolar potency (EC_{50} = 2 nM) (Goffin et al., 2018). The structure of BPAM538 in complex with the AMPA receptor GluA2 ligand-binding domain showed that BPAM538 belongs to the full-spanning class III of PAMs that occupy two allosteric binding sites per bound molecule (Frydenvang et al., 2022). In this study, we show that BPAM538 is also capable of modulating the kainate receptor GluK1 and report a 1.9 Å resolution X-ray structure of BPAM538 bound to the ligand-binding domain of the kainate receptor GluK1 with kainate.

2. Material and methods

2.1. Structure determination

The LBD of rat GluK1 (GluK1-LBD) was expressed and purified as previously described (Naur et al., 2005). Following purification, the protein was dissolved in 10 mM HEPES pH 7.0, 20 mM sodium chloride, and 1 mM EDTA. BPAM538 was synthesized as previously described (Goffin et al., 2018). A final GluK1-LBD concentration of 7.5 mg/mL was used in the presence of 12.7 mM kainate saturated with BPAM538. The protein solution was equilibrated at 6 °C for at least 24 h under rotation before setting up drops employing the hanging-drop vapor diffusion technique. A quantity of 500 µL of reservoir was added to each well in a 24-well VDX plate with sealant (Hampton Research). Each drop consisted of 1 µL of protein solution and 1 µL of reservoir solution (15.2 % PEG4000, 0.3 M lithium sulfate, and 0.1 M sodium acetate pH 5.5). Crystals harvested for data collection were briefly submerged into the reservoir solution supplemented with 10–20 % glycerol for cryoprotection and immediately flash-cooled in liquid nitrogen before storage.

X-ray diffraction data was collected at the BioMAX beamline, MAX IV Laboratory in Lund, Sweden (Ursby et al., 2020), and data was processed using XDS (Kabsch, 2010) and SCALA (Evans, 2006) in the CCP4 suite of programs (Winn et al., 2011). The structure was solved by molecular replacement in PHASER (McCoy et al., 2007) using the structure of GluK1-LBD in complex with kainate (PDB code: 4E0X) (Venskutonytė et al., 2012). Initial model building was performed using AUTOBUILD (Terwilliger et al., 2008) in PHENIX (Liebschner et al., 2019). During iterative rounds of model building in COOT (Emsley et al., 2010) and refinement in PHENIX, BPAM538, kainate, glycerol, ions, and water molecules were gradually built into the structure. The ligand coordinate file of BPAM538 was generated in MAESTRO (Maestro release 2021-3; Schrödinger, LLC, New York, NY, 2021). A restraint file for BPAM538 was generated using eLBOW (Moriarty et al., 2009), keeping the geometry from MAESTRO. Domain closures were calculated relative to a GluK1-LBD structure with an antagonist (PDB code: 3S2V, chain B) (Venskutonytė et al., 2011) employing the DynDom server (Hayward et al., 1998). Statistics for data collection and structure refinement are

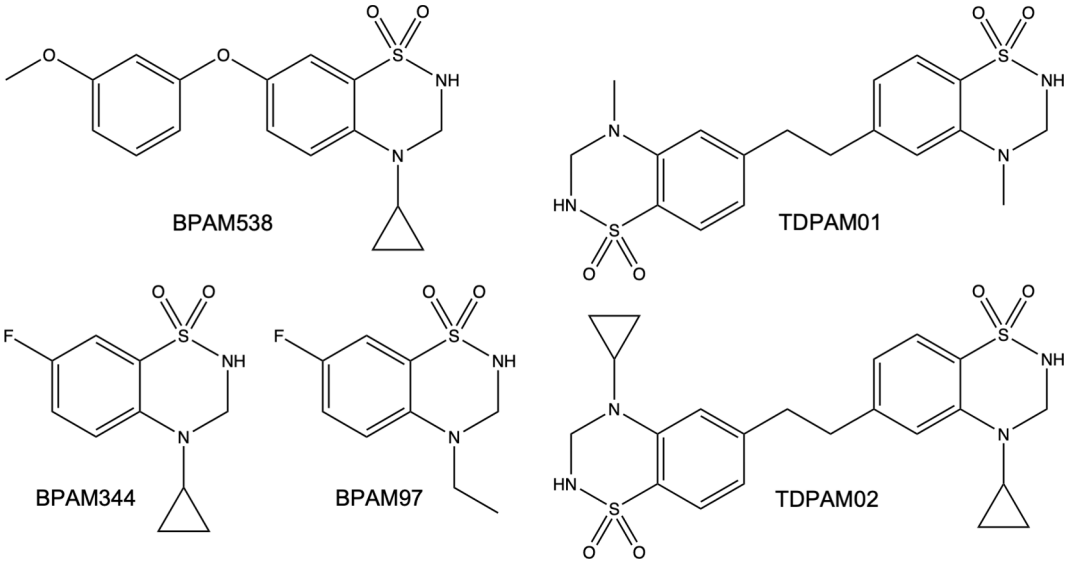

Fig. 2. Chemical structure of the positive allosteric modulators.

shown in Table 1. PyMOL (The PyMOL Molecular Graphics System, Version 2.5.4 Schrödinger, LLC) was used to prepare all structure figures.

2.2. Cell culturing and PAM activity assay

Grip Tite™ Human Embryonic Kidney (GT HEK293) (Invitrogen) cells were grown as previously described (Bay et al., 2024; Chałupnik et al., 2022,2023). For testing of PAM potentiation of agonist activity at GluK1$(Q)_b$ and GluK2$(VCQ)_a$, a Ca^{2+}-sensitive fluorescence-based assay was used. Briefly, in the absence and presence of PAMs, agonist-induced increases in fluorescence intensity from an intracellular Ca^{2+}-sensitive dye (Fluo8, AAT Bioquest) were measured in GluK1$(Q)_b$ and GluK2 $(VCQ)_a$ expressing cells cultured in 96-well plates using a FlexStation I plate reader (Molecular Devices).

All PAMs were dissolved in dimethyl sulfoxide (DMSO) and hereafter added to the assay buffer (100 mM choline chloride, 10 mM sodium chloride, 5 mM potassium chloride, 1 mM magnesium chloride, 20 mM calcium chloride, 10 mM HEPES, pH 7.4) on the day of the experiment. It was verified that DMSO concentrations up to 5 % had minimal effect on the agonist-induced response in GT HEK293 cells (data not shown). Attempts to improve the solubility of BPAM538 included the addition of DMSO (before and after the addition of BPAM538), pre-heating of BPAM538 stock solution for up to 45 min, assay buffer or compound solution (at least 15 min at 55 °C) as well as pre-incubation of BPAM538 in assay buffer added to the cells prior to recording. However, these modifications still did not allow the determination of potency at GluK1 $(Q)_b$.

Recordings of Ca^{2+} fluorescence were analyzed using SoftMax Pro software (version 5.4, Molecular Devices). Peak fluorescence response was calculated as the difference between baseline emission before agonist addition and the maximum emission after agonist addition. SigmaPlot was used to construct bar histograms shown as the mean response relative to BPAM344 (100 %) ± SEM from at least four independent experiments containing eight repetitions of 100 μM PAM per plate. Statistical analysis has been used to estimate the p-value between the application of kainate and co-application with the tested PAMs using the Student's *t*-test. A statistical difference is indicated with *** ($p < 0.001$) and not significant as ns.

2.3. Cell culture, transfection, and electrophysiology

HEK293T/17 (ATTC) cells were maintained in MEM containing GlutaMAX supplement. The media was supplemented with 10 % fetal bovine serum (Gibco). Cells were plated at a low density (1.6×10^4 cells/mL) on poly-D-lysine–coated, 35-mm plastic dishes and were transiently transfected 48 h later using the calcium phosphate technique, as previously described (Brown et al., 2016). After transfection, NBQX (30 μM) was added to the media to avoid cell death. All experiments were performed using cDNA from previous publications from the group (Brown et al., 2016).

Electrophysiology experiments were performed 48–72 h after washing off the transfection media. Agonist was rapidly applied to outside-out patches excised from transfected cells using a piezoelectric stack (Physik Instrumente). Solution exchange (10–90 % rise time of 250–350 μs) was determined by measuring the liquid junction current at the end of an experiment. All recordings were performed using an Axopatch 200B (Molecular Devices) with thick-walled, borosilicate glass pipettes (3–6 MΩ) coated with dental wax to reduce electrical noise. Series resistance (3–12 MΩ) was compensated by 95 %. Data was acquired using pClamp10 software (Molecular Devices) and tabulated using Excel (Microsoft Corp.). All experiments were performed at room temperature.

All chemicals were purchased from Sigma-Aldrich unless otherwise indicated. The external solution contained (in mM) 150 NaCl, 5 HEPES, and 0.1 $CaCl_2$, pH 7.3–7.4. The internal solution contained (in mM) 115 NaCl, 10 NaF, 5 HEPES, 5 Na_4BAPTA (Life Technologies), 1 $MgCl_2$, 0.5 $CaCl_2$, and 10 Na_2ATP, pH 7.3–7.4. The osmotic pressure of all solutions was adjusted to 295–300 mOsm with sucrose. Concentrated (10×) agonist stock solutions were prepared by dissolving L-Glu in the appropriate external solution and adjusting the pH to 7.3–7.4 and were stored at −20 °C. Stocks were thawed on the day of the experiment and used to prepare agonist-containing external solutions. BPAM344 and BPAM538 were dissolved in DMSO and stored at −20 °C as stock solution. Stocks were thawed to prepare solutions at the desired concentration on the day of the experiment.

Dose-response curves of BPAM538 were fitted using a single binding site isotherm function as described previously (Wong et al., 2006):

$$R = \frac{I_{max}}{1 + \left(\frac{EC_{50}}{[BPAM]}\right)^N}$$

where R is the response, EC_{50} is the concentration of BPAM538 that elicits half-maximal response and N is the slope.

Results are expressed as Mean ± SEM. Values for n refer to the number of individual patches. Statistical analysis was performed using Origin Pro 2020 (Originlab). The normality distribution of a population was tested using Shapiro-Wilk analysis, p-value > 0.15. For pairwise comparison groups we performed a two-tailed paired *t*-test on the populations where normal distribution assumption could not be rejected (Fig. 4B,C; Fig. 5C). For datasets that involved comparison between multiple groups (Fig. 4B), one-way ANOVA was performed with Tukey's HSD test. * indicates $p < 0.05$, ** $p < 0.01$, *** $p < 0.001$. All data was illustrated using Origin Pro 2020 and Adobe Illustrator CS5.

3. Results and discussion

3.1. X-ray structure of GluK1-LBD in complex with kainate and BPAM538

In crystals, GluK1-LBD forms a dimer in the presence of kainate (Plested et al., 2008; Venskutonytė et al., 2012), creating a dimer interface with two sites for allosteric modulators. Therefore, crystallization of BPAM538 in complex with GluK1-LBD was carried out in the presence of kainate. One GluK1-LBD dimer (chain A and chain B) was observed in the asymmetric unit of the crystal, with kainate bound at the orthosteric binding site in both subunits of the dimer (Fig. 1B). Kainate displays the same binding mode as previously observed (Plested et al., 2008; Venskutonytė et al., 2012). One chloride ion was seen at the dimer interface in agreement with previous structures of kainate receptors (Plested & Mayer, 2007) (Fig. 1B).

BPAM538 was observed to bind at the dimer interface with a single molecule occupying both allosteric binding sites (Fig. 1B–E). This defines BPAM538 as a class III PAM at kainate receptors, as previously observed at AMPA receptors (Frydenvang et al., 2022). Compared to the structure without BPAM538, the modulator seems to displace five binding-site water molecules. In comparison, BPAM344, belonging to class II (Frydenvang et al., 2022), binds with one molecule occupying each of the two pseudo-symmetric allosteric binding sites (Fig. 1E). Residues within 4 Å of the BPAM538 molecule include K531, P532, F533, M534, T535, S761, K762, L783, Q786, and L791 from chain A and can make van der Waals interactions (Fig. 1C). Nearly, the same residues are found within 4 Å of the modulator in chain B except for K531, L783, and L791. However, additional residues from chain B appear, which include I519 and G763 (Fig. 1C). Among these residues, the proline in position 532 from chain A is the only residue creating a hydrogen bond (2.8 Å) to the sulfonamide nitrogen atom of the modulator. Additionally, two water molecules in close vicinity of the modulator also make direct hydrogen bonds (2.0 and 3.3 Å, respectively) to one of the sulfonamide oxygen atoms in BPAM538. Five water molecules and a glycerol molecule were found close to the modulator but were not observed to generate any direct or polar contact.

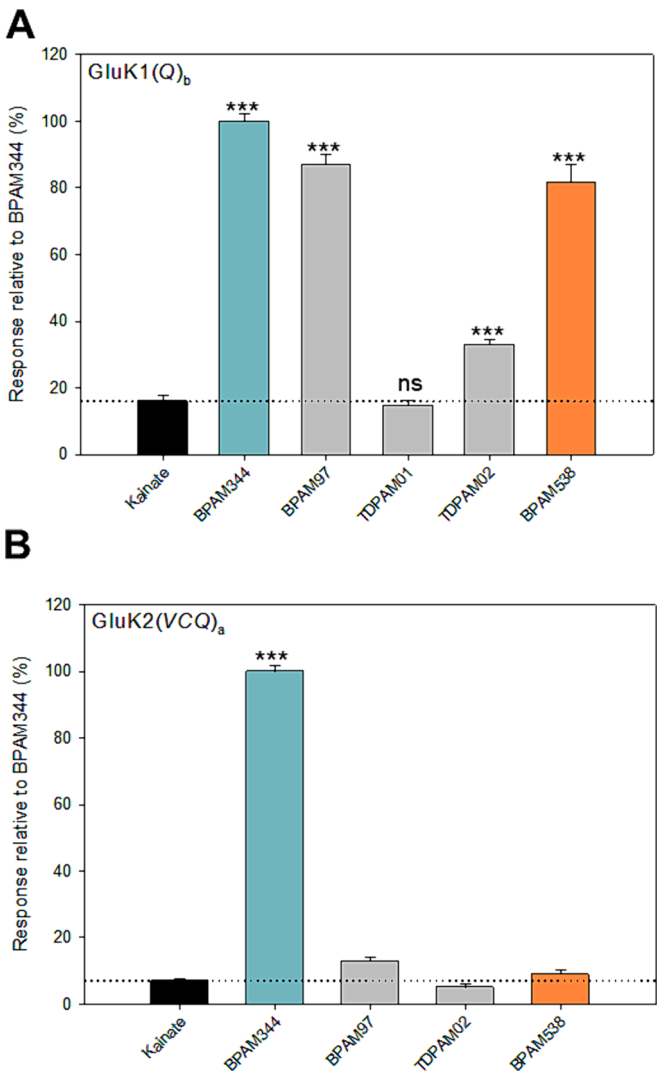

Fig. 3. Calcium-sensitive fluorescence-based assay. (A) Bar plots summarizing the response of GluK1(Q)$_b$ expressing cells to the agonist kainate (100 μM) in absence and presence of 100 μM concentration of BPAM344, BPAM97, TDPAM01, TDPAM02, and BPAM538. (B) Bar plots summarizing the response of GluK2(VCQ)$_a$ expressing cells to kainate (100 μM) in absence and presence of 100 μM concentration of BPAM344, BPAM97, TDPAM02, and BPAM538. Response values are shown normalized relative to the BPAM344 response. The bars presented are Means ± SEM of eight wells in at least four individual experiments. *** $p < 0.001$, ns = not significant.

Agonists are known to introduce domain closure in the LBD compared to the resting, unbound apo state of the receptor (Armstrong & Gouaux, 2000). As an apo structure is not available for GluK1, domain closures have previously been determined relative to an antagonist-bound structure (PDB code: 3S2V, chain B; Venskutonytė et al., 2011). The domain closure induced by kainate in GluK1-LBD was reported to be 25–28° (Møllerud et al., 2017). In the presence of BPAM538, the domain closure, as calculated in DynDom, is 24.9° and 25.5° in chains A and B, respectively (Fig. 1B). Thus, domain movements and agonist binding seem to be unaffected upon binding of BPAM538. In line with this, the distances between P532, P667, and R775 of chain A and B located at the interface of the dimer inside the allosteric binding site, the bottom of lobe D2, and the top of lobe D1, respectively, were calculated. Very similar distances were measured in the crystal structure of GluK1-LBD with kainate (PDB code: 4E0X) and upon binding of BPAM538 (9.2 Å vs 8.9 Å, 33.4 Å vs 32.0 Å, and 13.3 Å vs 13.4 Å). Therefore, BPAM538 is likely to diminish desensitization of GluK1 by stabilizing the dimer interface and not by affecting the domain closure.

Table 1
Crystal data, data collection, and refinement statistics of GluK1-LBD in complex with kainate and BPAM538.

	BPAM538
Crystal data	
PDB	8R36
Space group	$P4_12_12$
Unit cell axes a, b, c (Å)	71.49, 71.49, 232.90
Unit cell angles α, β, γ (°)	90, 90, 90
Molecules in a.u.[a]	2
Data collection	
Beamline	BioMAX, MAX IV, Lund, Sweden
Wavelength (Å)	0.976
Resolution (Å)	49.40–1.90 (2.00–1.90)[b]
No. of unique reflections	48,841 (6995)
Average redundancy	26.4 (26.6)
Completeness (%)	100 (100)
R_{merge} (%)	8.7 (45.7)
$I/\sigma I$	5.1 (1.5)
Wilson B (Å^2)	26.0
Refinement	
Amino acid residues (chain A/chain B)	254/254
Kainate/BPAM538	2/1
Chloride/sulfate/glycerol/water	8/4/4/358
R_{work}/R_{free} (%)	16.4/19.9
Average B values (Å^2) for:	
Amino acid residues (chain A/chain B)	35.6/36.4
Kainate/BPAM538	24.9/27.8
Chloride/sulfate/glycerol/water	62.5/72.0/54.6/38.7
R.M.S. deviation bond lengths (Å)/ angles (°)	0.0061/0.72
Ramachandran outliers/favored (%)	0.00/99.01
Rotamer outliers (%)/Cß outliers (%)/clash score	0.43/0.00/1.65

[a] a.u. is the asymmetric unit of the crystal.
[b] Numbers in parenthesis are for the outmost bin.

Superimposing the X-ray structure of GluA2-LBD complexed with L-Glu and BPAM538 (PDB code: 5OEW; Goffin et al., 2018) onto the GluK1-LBD structure with kainate and BPAM538 gave an RMSD value of 0.62 Å when imposed on lobe D1. BPAM538 also binds in a very similar manner in GluK1 and GluA2 (Fig. 1D). Similar interactions within 4 Å of BPAM538 and orientation of residues were observed between the AMPA and kainate receptor family. Of note, only two residues vary inside the binding region of BPAM538 (defined as residues within 4 Å of the modulator): (i) T535 in GluK1 that corresponds to GluA2 S518; in GluA2 S518 adopts two different side-chain conformations and (ii) Q786 in GluK1, which corresponds to N775 (flop) and S775 (flip) in GluA2. None of these residues form direct interaction with the modulator.

In comparison, a RMSD value of 0.12 Å was estimated on lobe D1 residues for GluK1-LBD with kainate and BPAM538 aligned with the X-ray structure of GluK1-LBD determined with kainate and BPAM344 (PDB code: 5MFQ; Larsen et al., 2017), indicating high similarity between the two structures. Taking a closer look at the binding pocket and the binding mode of the two modulators, residues located within 4 Å of the modulators adopt the same orientation and BPAM538 overlaps well with one of the two BPAM344 molecules (Fig. 1E). Noteworthy, a glycerol molecule located in proximity of BPAM538 seems to occupy the space where the second BPAM344 molecule is found; yet is not able to interact with the modulator (not shown).

In conclusion, the binding mode and interactions of BPAM538 at GluK1 correlate well with what has previously been observed at GluA2.

3.2. Functional screening of PAMs at kainate receptors

The observation that most PAMs work by occupying two identical binding sites in the LBD has stimulated the design and synthesis of

dimeric forms (Frydenvang et al., 2022). TDPAM02, belonging to class III, is one such example and is currently the most potent PAM at AMPA receptors known to date (Drapier et al., 2018).

We screened three class III PAMs (TDPAM01, TDPAM02, and BPAM538; Fig. 2) as well as two class II PAMs (BPAM97 and BPAM344, Fig. 2) for activity at GluK1(Q)$_b$ and GluK2(VCQ)$_a$. The ability of the PAMs to potentiate receptor response to 100 μM kainate was first evaluated in a single concentration of 100 μM at GluK1(Q)$_b$ using a calcium-sensitive fluorescence-based assay (Materials and Methods). Specifically, kainate activation of kainate receptors leads to an influx of Ca^{2+}, which increases intracellular Ca^{2+} concentration, which can be detected using an intracellular calcium-sensitive fluorescent dye. None of the tested PAMs appeared to be a better potentiator than the reference class II kainate receptor PAM BPAM344; however, BPAM97 within the same class II PAMs produced nearly similar response (87 % ± 3 %) as BPAM344 (100 % ± 2 %). As for the PAMs belonging to class III PAMs, only BPAM538 showed a modulatory effect at GluK1(Q)$_b$, potentiating the kainate response 5-fold (82 % ± 5 %) compared to (16 % ± 2 %) without PAM. TDPAM01 co-applied with kainate did not modulate GluK1(Q)$_b$ and TDPAM02 only weakly compared to BPAM344 (Fig. 3A). To address kainate receptor subtype preferences of the PAMs, BPAM538, TDPAM02, BPAM97, and BPAM344 were tested in the same manner at GluK2(VCQ)$_a$, which showed that only BPAM344 was observed to potentiate the response of kainate (Fig. 3B).

In summary, BPAM538 and BPAM97 showed a preference for the GluK1(Q)$_b$ receptor subtype, and characterization of the functional profile (EC_{50}) was attempted using the calcium-sensitive fluorescence-based assay. However, due to the poor solubility of BPAM538 (Goffin et al., 2018) in the assay buffer, it was impossible to determine the EC_{50} value at GluK1(Q)$_b$ using this assay.

3.3. Electrophysiology recordings with BPAM538

Next, the positive allosteric effect of BPAM344 and BPAM538 was studied in electrophysiology recordings of outside-out patches excised from HEK293 cells expressing either the homomeric kainate receptors, GluK1(Q)$_b$ or GluK2(VCQ)$_a$, or the homomeric AMPA receptor GluA2(Q)$_i$ (Figs. 4 and 5) as described previously (Bowie et al., 2003). Due to low expression levels observed with GluK1(Q)$_b$, cells transfected with cDNA for kainate receptors were co-transfected with the auxiliary subunit, NETO2, to enhance surface expression (Copits et al., 2011). In all cases, agonist-evoked membrane currents elicited by 10 mM L-Glu, 250

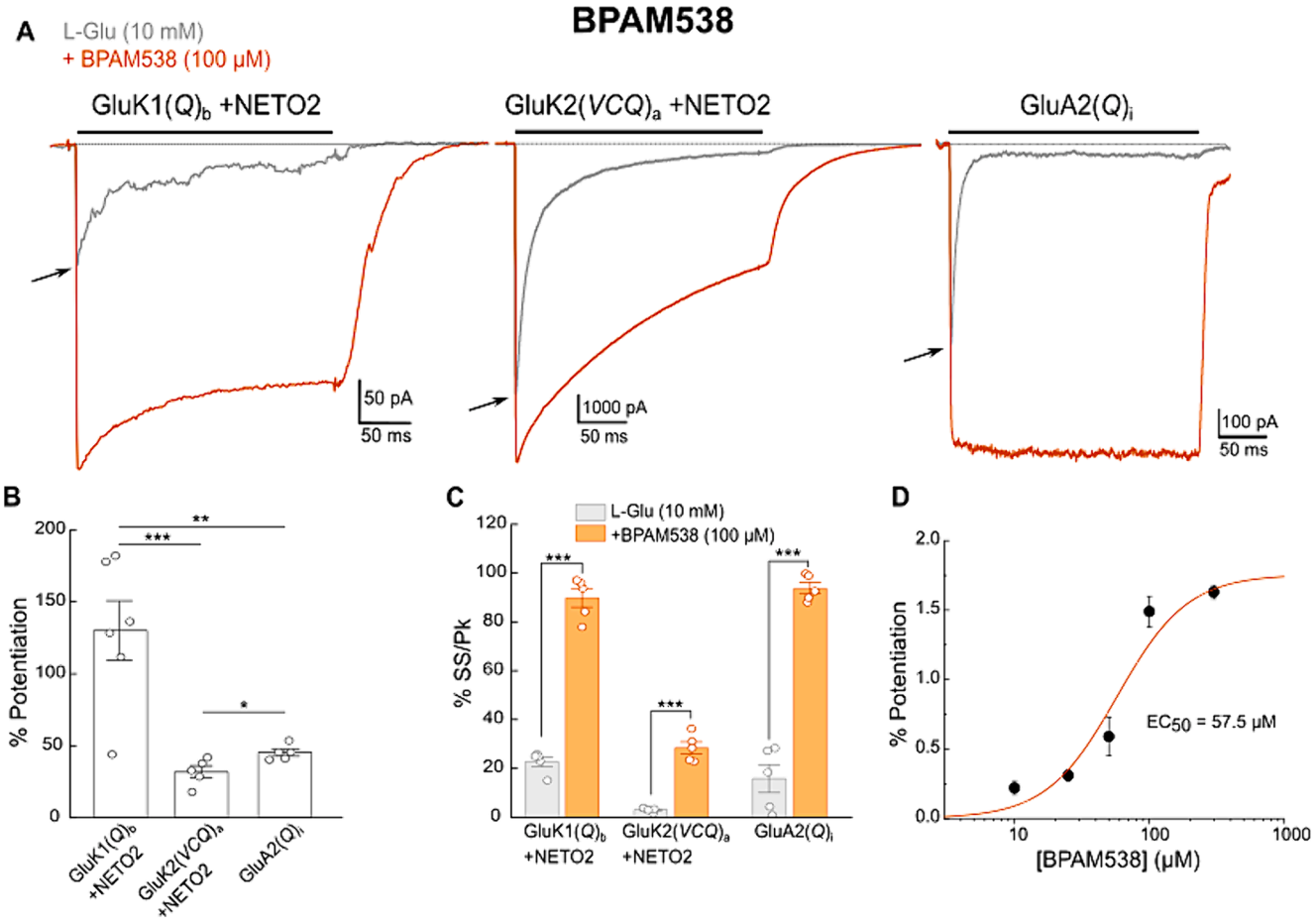

Fig. 4. BPAM538 increases the peak response amplitude and slows the onset of GluK1(Q)$_b$, GluK2(VCQ)$_a$, and GluA2(Q)$_i$ receptor desensitization. A) Representative current traces for GluK1(Q)$_b$, GluK2(VCQ)$_a$, and GluA2(Q)$_i$ receptors in response to 250 ms application of 10 mM L-Glu alone (gray) and following pre-incubation with 100 μM BPAM538 (orange, Patch #s 24516039, 24514024, and 24530016, respectively). GluK1(Q)$_b$ and GluK2(VCQ)$_a$ receptors were co-expressed with NETO2. Arrows point to peak current amplitude in response to L-Glu alone. Black bar represents the 250 ms agonist application period. B) Percent increase in the peak amplitude response (potentiation) to 10 mM L-Glu following pre-incubation with 100 μM BPAM538. Data presented as Mean ± SEM, with each data point corresponding to one patch. $F(2,15) = 15.63$, $p < 0.001$, one-way ANOVA. Tukey's HSD test, *** $p < 0.001$, ** $p < 0.01$, * $p < 0.05$. C) Steady-state (SS) current amplitude as a percentage of the peak response (Pk) for the 10 mM L-Glu response alone (grey bars) or following pre-incubation with 100 μM BPAM538 (orange bars). *** $p < 0.001$, two-tailed paired t-test. Data presented as Mean ± SEM, with each data point corresponding to one patch recording. D) Agonist dose–response curve in the presence of different concentrations (10–300 μM) of BPAM538. (For interpretation of the references to colour in this figure legend, the reader is referred to the web version of this article.)

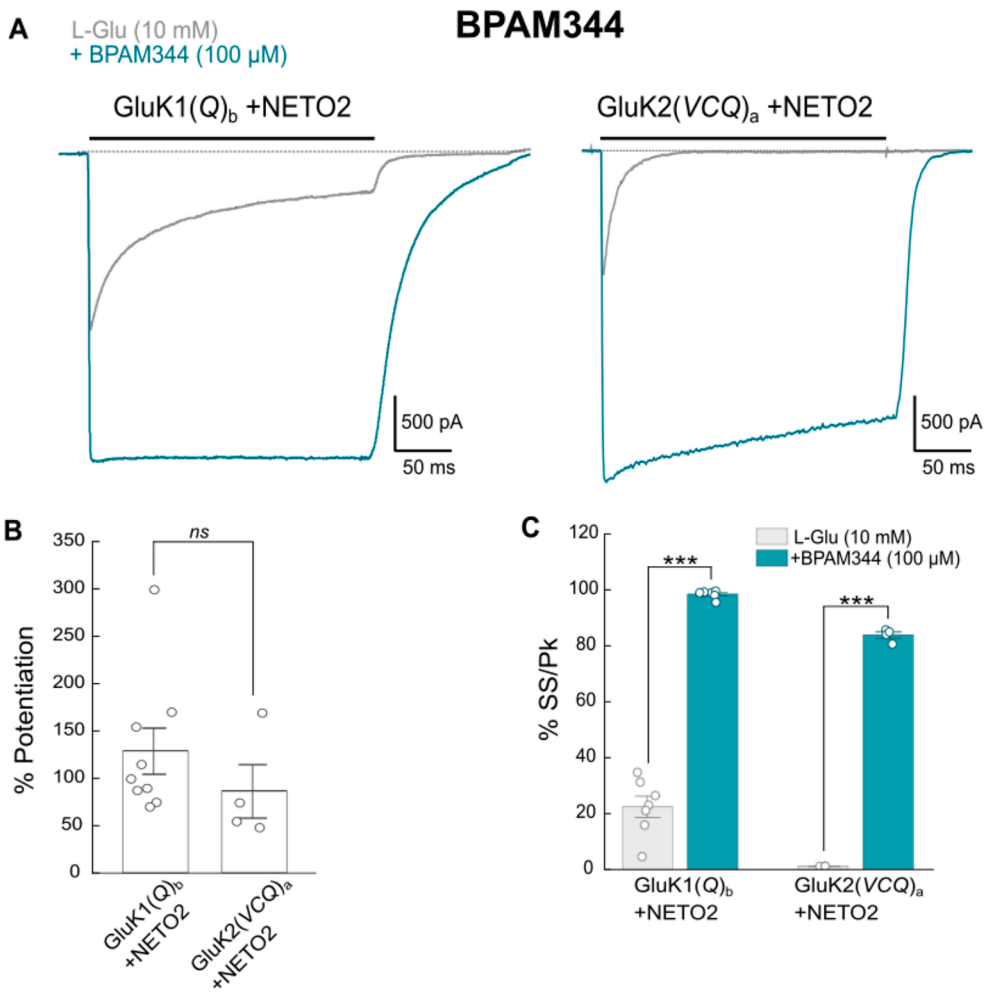

Fig. 5. BPAM344 increases the peak response amplitude and slows the onset of GluK1(Q)$_b$ and GluK2(VCQ)$_a$ receptor desensitization. (A) Representative current traces for GluK1(Q)$_b$ and GluK2(VCQ)$_a$ receptors co-expressed with NETO2 in response to 250 ms application of 10 mM L-Glu alone (gray) and following pre-incubation with 100 μM BPAM344 (teal, Patch #s 24,510,019 and 24,510,002, respectively). Black bar represents the 250 ms agonist application period. (B) Percent increase in the peak amplitude response (potentiation) to 10 mM L-Glu following pre-incubation with 100 μM BPAM344. Two-tailed unpaired *t*-test with Welch correction, ns = no statistical significance (GluK1(Q)$_b$: 129 ± 24 %, n = 9; GluK2(VCQ)$_a$: 87 ± 28 %, n = 4). C) Steady-state/peak response ratio (SS/Pk %) observed with 10 mM L-Glu alone (gray bars) and following pre-incubation of 100 μM BPAM344 (teal bars). *** $p < 0.001$, two-tailed paired *t*-test. Data presented as Mean ± SEM, with each data point corresponding to one patch recording.

ms duration, Hp, −100 mV) were rapidly rising within the first few milliseconds and declined from the peak response due to the onset of desensitization (Figs. 4A and 5A).

Following pre-incubation with either 100 μM BPAM344 or BPAM538, the peak response increased in amplitude, and channel kinetics exhibited a slowing of desensitization onset (Figs. 4A and 5A, Table 2). BPAM538 increased the peak response of GluK1(Q)$_b$ (130 ± 21 %, n = 6) significantly more than GluK2(VCQ)$_a$ receptors (32 ± 4 %, n = 5) (one-way ANOVA with Tukey's HSD; $p < 0.001$) (Fig. 4A,B). BPAM538 also increased the peak response of GluA2(Q)$_i$ responses by 46 ± 2 % (n = 5) (Fig. 4A,B), demonstrating that its ability to regulate channel gating is shared amongst kainate and AMPA receptors. BPAM344 also increased the peak amplitude of GluK1(Q)$_b$ and GluK2(VCQ)$_a$ responses by 129 ± 24 % (n = 9) and 87 ± 28 % (n = 4), respectively (Fig. 5A,B).

The rate of onset of desensitization was determined by measuring the steady-state/peak response ratio (SS/Pk %), which reports the degree of decline in the peak response after a long, 250 ms agonist application (Table 2). As noted during the functional screening, BPAM538 had a more potent effect on GluK1(Q)$_b$ and GluA2(Q)$_i$ than GluK2(VCQ)$_a$ with

Table 2
Increase in peak response and slowing of desensitization onset following pre-incubation with either 100 μM BPAM538 or BPAM344.

Ligand	GluK1(Q)$_b$ + NETO2			GluK2(VCQ)$_a$ + NETO2			GluA2(Q)$_i$		
	Pk[a] (%)	SS/Pk[b] (%)	n	Pk[a] (%)	SS/Pk[b] (%)	n	Pk[a] (%)	SS/Pk[b] (%)	n
L-Glu		23 ± 2	6		2.9 ± 0.4	5		16 ± 6	5
L-Glu+BPAM538	130 ± 21	90 ± 4	6	32 ± 4	28 ± 3	5	46 ± 2	94 ± 2	5
L-Glu		22 ± 4	9		1.1 ± 0.1	4			
L-Glu + BPAM344	129 ± 24	98 ± 1	9	87 ± 28	84 ± 1	4			

[a] Peak.
[b] Steady-state/peak ratio.

percentage steady-state/peak response ratios of 90 ± 4 % (n = 6) and 94 ± 2 % (n = 5), respectively compared to 28 ± 3 % (n = 5; two-tailed paired t-test, GluK1(Q)$_b$ $p < 0.001$, GluK2(VCQ)$_a$ $p < 0.001$, and GluA2(Q)$_i$ $p < 0.001$) (Fig. 4A,C). Separate dose–response relationship experiments on GluK1(Q)$_b$ estimated the EC_{50} of BPAM538 to be 58 ± 29 μM with a Hill coefficient of 1.7 ± 0.7 (n = 4) (Fig. 4D). The EC_{50} of BPAM538 at GluA2(Q)$_i$ has previously been determined to 2 nM (Goffin et al., 2018), and therefore, BPAM538 can be considered an AMPA receptor preferring PAM like BPAM344.

In contrast, the positive allosteric effect of BPAM344 did not discriminate between GluK1(Q)$_b$ and GluK2(VCQ)$_a$ with the percentage steady-state/peak response ratios estimated to be 98 ± 1 % (n = 9) and 84 ± 1 % (n = 4), respectively (Fig. 5A,C).

3.4. Concluding remarks

In this study, we have determined the structure of the LBD of GluK1 in complex with kainate and BPAM538. We demonstrate that a small molecule PAM belonging to class III, manifested as one of the most potent AMPA receptor PAMs, can also modulate GluK1 expressed in HEK293 cells. On the other hand, weak potentiation of GluK2 was observed, indicating that it should be possible to achieve selective modulation of kainate receptor subunits. The structural and functional insight into the new PAM class at kainate receptors provides an improved basis for future design of PAMs with selectivity at kainate receptors.

Funding

The Lundbeck foundation (R264-2017-3416) (S.M.F, J.S.K.), the Independent Research Fund Denmark – Medical Sciences (0134-00162B) (Y.B., J.S.K.), Danscatt (Y.B., S.M.F., K.F., J.S.K.), and the Canadian Institutes of Health Research (FRN 163317) (D.B.) are acknowledged for financial support. We acknowledge MAX IV Laboratory for time on Beamline BioMAX under Proposal 20200259. Research conducted at MAX IV, a Swedish national user facility, is supported by the Swedish Research council under contract 2018-07152, the Swedish Governmental Agency for Innovation Systems under contract 2018-04969, and Formas under contract 2019-02496.

CRediT authorship contribution statement

Yasmin Bay: Conceptualization, Formal analysis, Investigation, Methodology, Validation, Writing – original draft. **Federico Javier Miguez Cabello:** Formal analysis, Investigation, Methodology, Writing – review & editing. **Chloe C. Koens:** Formal analysis, Investigation, Methodology, Writing – review & editing. **Stine M. Frantsen:** Conceptualization, Investigation, Methodology. **Darryl S. Pickering:** Conceptualization, Investigation, Methodology, Supervision. **Karla Frydenvang:** Formal analysis, Investigation, Supervision, Validation, Writing – review & editing. **Pierre Francotte:** Resources, Writing – review & editing. **Bernard Pirotte:** Resources, Writing – review & editing. **Anders Skov Kristensen:** Methodology, Supervision, Validation, Writing – review & editing. **Derek Bowie:** Conceptualization, Funding acquisition, Methodology, Supervision, Validation, Writing – review & editing. **Jette Sandholm Kastrup:** Conceptualization, Formal analysis, Funding acquisition, Methodology, Supervision, Validation, Writing – original draft, Writing – review & editing.

Declaration of competing interest

The authors declare that they have no known competing financial interests or personal relationships that could have appeared to influence the work reported in this paper.

Data availability

Data will be made available on request.

Acknowledgements

MAX IV, Lund, Sweden is thanked for providing beamtime and technical assistance. Heidi Peterson is thanked for producing the GluK1-LBD protein.

References

Armstrong, N., Gouaux, E., 2000. Mechanisms for activation and antagonism of an AMPA-sensitive glutamate receptor: crystal structures of the GluR2 ligand binding core. Neuron 28, 165–181. https://doi.org/10.1016/s0896-6273(00)00094-5.

Bay, Y., et al., 2024. Small molecule positive allosteric modulation of homomeric kainate receptors GluK1-3: development of screening assays and insight into GluK3 structure. FEBS J. 291, 1506–1529. https://doi.org/10.1111/febs.17046.

Bowie, D., et al., 2003. Allosteric regulation and spatial distribution of kainate receptors bound to ancillary proteins. J. Physiol. 547, 373–385. https://doi.org/10.1113/jphysiol.2002.033076.

Brown, P.M., et al., 2016. Kainate receptor pore-forming and auxiliary subunits regulate channel block by a novel mechanism. J. Physiol. 594, 1821–1840. https://doi.org/10.1113/JP271690.

Chałupnik, P., et al., 2022. Discovery of the first highly selective antagonist of the GluK3 Kainate receptor subtype. Int. J. Mol. Sci. 23, 8797. https://doi.org/10.3390/ijms23158797.

Chałupnik, P., et al., 2023. Structure-activity relationship and solubility studies of N1-substituted quinoxaline-2,3-diones as kainate receptor antagonists. ChemMedChem 18, e202300278.

Contractor, A., et al., 2011. Kainate receptors coming of age: milestones of two decades of research. Trends Neurosci. 34, 154–163. https://doi.org/10.1016/j.tins.2010.12.002.

Copits, B.A., et al., 2011. Synaptic targeting and functional modulation of GluK1 kainate receptors by the auxiliary Neuropilin and Tolloid-Like (NETO) proteins. J. Neurosci. 31, 7334–7340. https://doi.org/10.1523/JNEUROSCI.0100-11.2011.

Drapier, T., et al., 2018. Enhancing action of positive allosteric modulators through the design of dimeric compounds. J. Med. Chem. 61, 5279–5291. https://doi.org/10.1021/acs.jmedchem.8b00250.

Emsley, P., et al., 2010. Features and development of Coot. Acta Crystallogr. D Biol. Crystallogr. 66 (Pt 4), 486–501. https://doi.org/10.1107/s0907444910007493.

Evans, P., 2006. Scaling and assessment of data quality. Acta Crystallogr. D Biol. Crystallogr. 62, 72–82. https://doi.org/10.1107/s0907444905036693.

Frydenvang, K., et al., 2022. Structural basis for positive allosteric modulation of AMPA and kainate receptors. J. Physiol. 600, 181–200. https://doi.org/10.1113/jp280873.

Goffin, E., et al., 2018. 7-Phenoxy-substituted 3,4-dihydro-2H-1,2,4-benzothiadiazine 1,1-dioxides as positive allosteric modulators of α-amino-3-hydroxy-5-methyl-4-isoxazolepropionic acid (AMPA) receptors with nanomolar potency. J. Med. Chem. 61, 251–264. https://doi.org/10.1021/acs.jmedchem.7b01323.

Hansen, K.B., et al., 2021. Structure, function, and pharmacology of glutamate receptor ion channels. Pharmacol. Rev. 73, 298–487. https://doi.org/10.1124/pharmrev.120.000131.

Hayward, S., Berendsen, H.J., 1998. Systematic analysis of domain motions in proteins from conformational change; new results on citrate synthase and T4 lysozyme. Proteins 30, 144–154.

Jin, R., et al., 2005. Mechanism of positive allosteric modulators acting on AMPA receptors. J. Neurosci. 25, 9027–9036. https://doi.org/10.1523/JNEUROSCI.2567-05.2005.

Kabsch, W., 2010. XDS. Acta Crystallogr. D Biol. Crystallogr. 66, 125–132. https://doi.org/10.1107/s0907444909047337.

Larsen, A.P., et al., 2017. Identification and structure-function study of positive allosteric modulators of kainate receptors. Mol. Pharmacol. 91, 576–585. https://doi.org/10.1124/mol.116.107599.

Lerma, J., Marques, J.M., 2013. Kainate receptors in health and disease. Neuron 80, 292–311. https://doi.org/10.1016/j.neuron.2013.09.045.

Liebschner, D., et al., 2019. Macromolecular structure determination using X-rays, neutrons and electrons: recent developments in Phenix. Acta Crystallogr. D Struct. Biol. 75 (Pt 10), 861–877. https://doi.org/10.1107/s2059798319011471.

McCoy, A.J., et al., 2007. Phaser crystallographic software. J. Appl. Crystallogr. 40, 658–674. https://doi.org/10.1107/s0021889807021206.

Moriarty, N.W., et al., 2009. electronic Ligand Builder and Optimization Workbench (eLBOW): a tool for ligand coordinate and restraint generation. Acta Crystallogr. D Biol. Crystallogr. 65, 1074–1080. https://doi.org/10.1107/S0907444909029436.

Møllerud, S., et al., 2017. Lessons from crystal structures of kainate receptors. Neuropharmacology 112(Pt A), 16-28. https://doi/10.1016/j.neuropharm.2016.05.014.

Naur, P., et al., 2005. Crystal structure of the kainate receptor GluR5 ligand-binding core in complex with (S)-glutamate. FEBS Lett. 579, 1154–1160. https://doi.org/10.1016/j.febslet.2005.01.012.

Plested, A.J., et al., 2008. Molecular basis of kainate receptor modulation by sodium. Neuron 58, 720–735. https://doi.org/10.1016/j.neuron.2008.04.001.

Plested, A.J., Mayer, M.L., 2007. Structure and mechanism of kainate receptor modulation by anions. Neuron 53, 829–841. https://doi.org/10.1016/j.neuron.2007.02.025.

Puja, G., et al., 2022. Benzothiadiazines derivatives as novel allosteric modulators of kainic acid receptors. J. Physiol. Pharmacol. 73 https://doi.org/10.26402/jpp.2022.1.02.

Sobolevsky, A.I., et al., 2009. X-ray structure, symmetry and mechanism of an AMPA-subtype glutamate receptor. Nature 462, 745–756. https://doi.org/10.1038/nature08624.

Sun, Y., et al., 2002. Mechanism of glutamate receptor desensitization. Nature 417 (6886), 245–253. https://doi.org/10.1038/417245a.

Tee, W.V., Berezovsky, I.N., 2024. Allosteric drugs: New principles and design approaches. Curr. Opin. Struct. Biol. 84, 102758 https://doi.org/10.1016/j.sbi.2023.102758.

Terwilliger, T.C., et al., 2008. Iterative model building, structure refinement and density modification with the PHENIX AutoBuild wizard. Acta Crystallogr. D Biol. Crystallogr. 64, 61–69. https://doi.org/10.1107/s090744490705024x.

Traynelis, S.F., et al., 2010. Glutamate receptor ion channels: structure, regulation, and function. Pharmacol. Rev. 62, 405–496. https://doi.org/10.1124/pr.109.002451.

Ursby, T., et al., 2020. BioMAX – the first macromolecular crystallography beamline at MAX IV Laboratory. J. Synchrotron Rad. 27 (Pt 5), 1415–1429. https://doi.org/10.1107/S1600577520008723.

Venskutonytė, R., et al., 2011. Selective kainate receptor (GluK1) ligands structurally based upon 1H-cyclopentapyrimidin-2,4(1H,3H)-dione: synthesis, molecular modeling, and pharmacological and biostructural characterization. J. Med. Chem. 54, 4793–4805. https://doi.org/10.1021/jm2004078.

Venskutonytė, R., et al., 2012. Kainate induces various domain closures in AMPA and kainate receptors. Neurochem. Int. 61, 536–545. https://doi.org/10.1016/j.neuint.2012.02.016.

Winn, M.D., et al., 2011. Overview of the CCP4 suite and current developments. Acta Crystallogr. D Biol. Crystallogr. 67 (Pt 4), 235–242. https://doi.org/10.1107/s0907444910045749.

Wong, A.Y., et al., 2006. External ions are coactivators of kainate receptors. J. Neurosci. 26, 5750–5755. https://doi.org/10.1523/JNEUROSCI.0301-06.2006.